POLITECNICO
MILANO 1863

SCUOLA DI INGEGNERIA INDUSTRIALE
E DELL'INFORMAZIONE

Executive Summary of the Thesis

Reversible Turbomachinery for Energy Storage Applications

Laurea Magistrale in Mechanical Engineering - Ingegneria Meccanica

Author: Matteo Pozzi

Advisor: Prof. Alessandro Romei

Academic year: 2022-2023

1. Introduction

More and more in the following years, renewable energy sources will play an increased role in the energy mix for Europe and for the entire world. The European Union (EU) has set different targets and plans to reduce greenhouse gas emissions by 55% by 2030 and to become the first climate-neutral continent by 2050 [1]. In order to make this possible, the share of renewable sources in the energy mix has to be increased. The natural variability of these type of source has to be accompanied with an increased number of storage systems, with the target of 200 GW by 2030 and 600 GW by 2050.
Energy storage systems differ by the power size, discharge time and efficiency. Some systems are more suitable to provide temporary peak power, while others are more adapt for covering the baseline demand, due to the increased discharge time. Another way to characterise this type of system is its efficiency of a storage system. It is defined as the ratio between the energy discharged and the energy accumulated during charge. It is called the Round Trip Efficiency (RTE):

$$RTE = \frac{W_{dis}}{W_{ch}} \tag{1}$$

A developing storage system that operates for large powers, with a discharge time in the order of hours, is Pumped Thermal Energy Storage (PTES). This system operates via a closed reversible Brayton cycle. During charge, it acts as a heat pump, transferring heat from a cold storage to a hot one, while during discharge it uses the heat accumulated to run a turbine and generate electricity.
An ideal Brayton cycle is completely reversible, as shown in Figure 1.

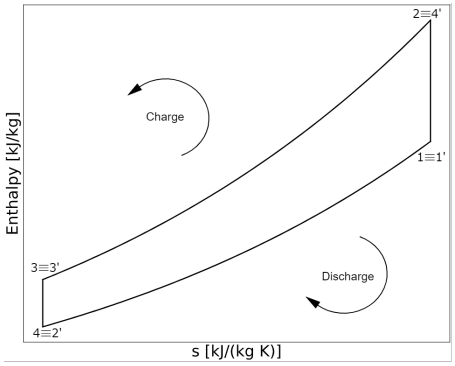

Figure 1: Ideal reversible Brayton cycle.

This is a captivating feature of this type of plant, because it means that ideally RTE is equal to 1. However, when considering a real cycle, pressure losses in the heat exchangers and turbomachinery irreversibilities are present and forces the direct and reverse cycle to differ.
An example of the real cycles for charge and

discharge is shown in Figure 2.

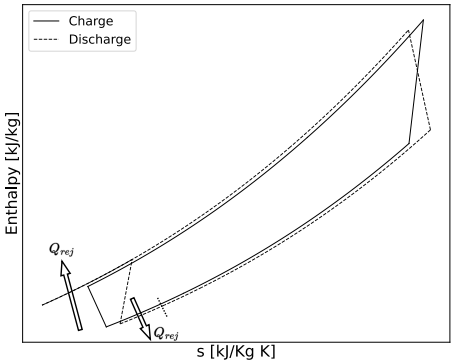

Figure 2: Real Brayton charge and discharge cycles.

The pressure ratio of discharge mode is higher than the one of charge mode, and the discharge cycle presents two heat rejections to discharge the heat from the irreversibilities [2].
The driving factor in energy storage systems is, as Laughlin stated, "safety, low cost and high efficiency, in this order" [3]. This type of technology does not introduce safety issues that are not known, since it utilises well-proven components, such as turbomachinery and heat exchangers. A way to reduce a big part of the costs [4] is to exploit the (quasi) symmetry of the two thermodynamic cycles to use reversible turbomachinery that carry out the compressions and expansions. In this way, the plant is considerably simplified and the cost for only two machines has to be sustained.
However, having the same geometry for both operating modes presents some challenges.
First of all the thermodynamic operating conditions are not the same, as already stated, therefore a different amount of work is exchanged for the two modes. This means that a different density variation throughout the machine is experienced. The density variation should be matched by the changes in the passage height to keep the axial velocity constant. Since this variation is not the same between compressor and turbine mode, one of the two cannot have constant axial velocity and therefore repeating stages. Moreover, different axial velocity means that one of the two modes operates with incidence angles different that the design ones. [2] [5]
Aim of this work is to design a machine that optimises both compressor and turbine mode. It is decided to develop a code based on a mean-line approach for the calculations of the thermo-fluidynamic parameters. Compressor mode, being more sensible to incidence angle variation, is designed at its optimum condition, and using a repeated stages approach. Turbine mode, instead, is analysed, running the geometry obtained from the compressor code backwards to calculate its performances. These calculations are integrated with high-fidelity computational fluid dynamics (CFD) to validate the model and to analyse the flow field. Finally, if the mean-line model is accurate, the codes are coupled with an optimisation routine, which is able to find the geometry that maximises both functioning modes. The maximisation is not intended in terms of single machine η_{is}, but in terms of RTE of the whole plant.
Two types of machine architectures are considered, one composed by only rotors and stators, using repeated stages for the middle ones. The other substitutes first and last stage of the previous architecture with guide vanes. This choice simplifies the design, since only repeating stages are present. The comparison allows to study if a kind of architecture is more suitable for this kind of application.
The machines performance are calculated using either nitrogen N_2 or argon Ar. Ar, being monoatomic, has a higher capacity ratio γ than N_2. This means that the same temperature ratio can be achieved with a lower pressure ratio, therefore a lower number of stages N_{st} for Ar, as shown in Figure 3

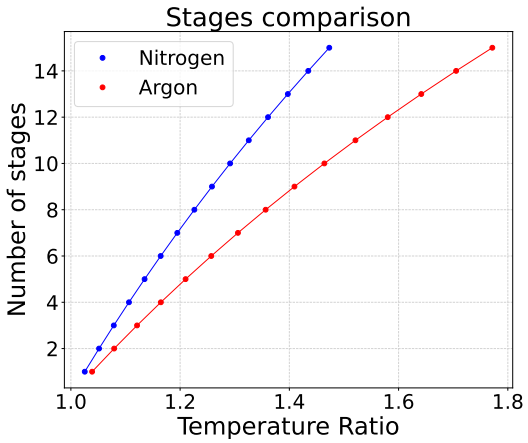

Figure 3: Number of stages vs temperature ratio comparison for N_2 and Ar.

However, the heat exchanger would be more

costly because Ar is a monoatomic gas, therefore it is still unclear which fluid would be more appropriate for PTES and both deserve to be investigated.

2. Meanline Analysis

Two codes are developed, one for the compressor mode, the other for the turbine mode. As said, the compressor one is a design code, which generates the geometry starting from input parameters, such as adimensional coefficients, thermodynamic boundary conditions and geometrical parameters. The turbine code, instead, is an analysis code, it takes as input the geometry from the compressor and run it backwards to calculate the performance.

The input parameters for the compressor code are:

- P_{Tin}, T_{Tin} and P_{Tout}
- flow coefficient ϕ for first, middle and last stage
- work coefficient λ for first and last stage
- reaction degree χ for first and last stage
- mean diameter D_m
- solidity σ for all the cascades
- chord Reynolds number Re_c for all the cascades
- mass flow rate $\dot{m}$
- number of stages N_{st}

The code is being written in order to run with general equations of state, which are not limited to the type of fluid. Fluid properties are calculated through CoolProp library, which implements state of the art equations of state for characterizing the fluid behaviour.

The code starts from the inlet station and then progresses throughout the machine to calculate thermo-fluidynamic properties at each successive station. For every calculation step, the quantities calculated have to respect the fluidynamic (in terms of velocity triangles), the thermodynamic (in terms of entropy generated from the losses) and mass conservation. A *while* loop is performed until the difference between a chosen quantity (entropy) for two consecutive iterations is under a given absolute tolerance.

The meanline code reliability depends on the accuracy of loss and angle correlations, i.e. optimal incidence i_{opt} and deviation angle δ.

Compressor losses are taken from Aungier [6], who revised existing correlations. They are split in different contributions:

- profile losses $\bar{\omega}_{prof}$
- secondary flow losses $\bar{\omega}_{sec}$
- end-wall losses $\bar{\omega}_{ew}$
- tip-clearance losses $\bar{\omega}_{tip}$

Shock-losses are not accounted for due to the low-loading nature of this application. Losses are defined in terms of total pressure loss with respect to the inlet kinetic energy, in the frame of reference of the cascade of interest:

$$\bar{\omega} = \frac{P_{Tin} - P_{Tout}}{P_{Tin} - P_{in}} \tag{2}$$

i_{opt} and δ are taken as well from Aungier [6].

After completing the calculations, the flow is distributed along the radial coordinate using a free-vortex approach, assuming ideal radial equilibrium. The flow deflections ϵ are checked with the Howell's limit along the whole span.

The last step is the blade geometry creation: starting from the flow angles, the blade angles are calculated using i_{opt} and δ and chord c is obtained from the target Re_c. The blade profile chosen is the double circular arc (DCA), which is symmetric, therefore suitable for both flow directions.

Turbine code takes as input only P_{Tin}, T_{Tin} and $\dot{m}$. It analyses the flow, given the compressor geometry taken in the opposite direction.

Turbine losses are taken from Aungier [7] and split in different contribution:

- profile losses $\bar{\omega}_{prof}$
- trailing-edge losses $\bar{\omega}_{TE}$
- secondary-flow losses $\bar{\omega}_{sec}$
- tip-clearance losses $\bar{\omega}_{tip}$

As for compressors, shock losses are not considered.

δ correlation is taken from Aungier [7] as well.

In order to trust the meanline codes, they have to be validated, comparing them with high-fidelity CFD simulations. Once they can be trusted, they can be coupled with an optimisation routine to find the machine that maximises the functioning for both ways of operation.

The validation is performed with the rotors and stators machine, since different type of stages are represented. The machine used presents not excessive loading ($\lambda < 0.4$) and it is composed by only three stages, in order to avoid the repetition of the middle stages. The adimensional input parameters are shown in Table 1.

Table 1: Input values for the preliminary performance prediction.

Stage	Row	ϕ	λ	χ	σ	Re_c
1	R	0.55	0.4	0.85	1.2	4.5e5
	S				1	4e5
2	R	0.62	/	0.5	1.25	4.5e5
	S					
3	R	0.62	0.22	0.68	1	4.3e5
	S				1.2	4.3e5

P_{Tin} is chosen as 2 bar, T_{Tin} as 300K and P_{Tout} as 2.65. In this way β_{TT} is of 1.325, meaning an average β for every stage of 1.098. The mean diameter D_m is chosen as 1080 mm and working fluid is air. λ for the repeated stages resulted 0.333. The validation is first performed on quasi-3D simulations of a single blade to analyse the midspan fluidynamic, then on of the whole machine, to account for 3D effects, such as tip clearance and secondary flows.
Quasi-3D simulations were performed simulating only a blade slab at midspan, in order to verify the fluidynamic. The limits in radial direction followed the change in passage height of the full blade, in order to match the meridional velocity. An example for the mesh of a single blade is shown in Figure 4.

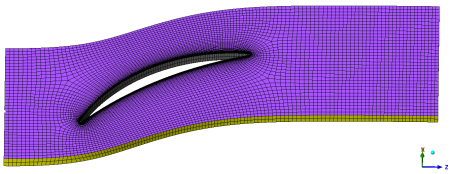

Figure 4: Mesh example for a single compressor rotor blade.

2D simulations could not be performed, since the meshing software (Turbogrid) forces to have at least two elements in radial direction. That is the reason because it is chosen a quasi-3D approach, forcing the streamtube width by using free-slip condition on the faces perpendicular to the radial direction.
It is chosen to simulate the second rotor blade, being a simpler cascade, having $\chi = 0.5$. The number of elements resulted from grid independency was of 100 000, which means only the half, 50 000 in the blade-to-blade plane.
The simulation resulted accurate, with an error on the thermo-fluidynamic quantities lower than 5%.
Simulations of the whole machine required the discretisation on the radial coordinate, which has to account for boundary layer effects and tip clearance. The number of cells for a single blade increase to about 2 000 000.
In this case, the meanline code predicted well the fluidynamic until the second stator, where an error in the calculation of the deviation angle resulted in non-accuracy of the flow characteristics also for the successive cascades. This effect is depicted in Figure 5.

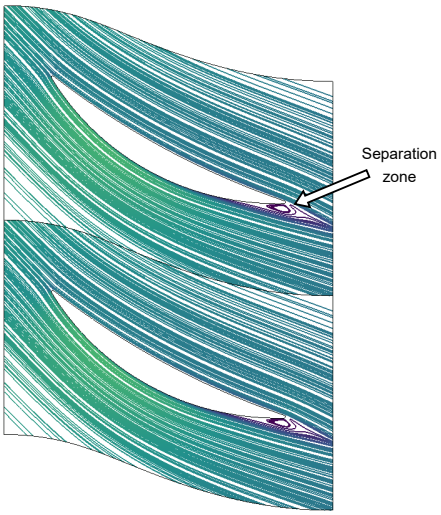

Figure 5: Separation zone for the second stator

Nevertheless, P_{Tout} and η_{is} resulted, respectively, 262 055 Pa and 90.5%, both matching the meanline code with a percentage error of the 1%. Turbine is then analysed as well, reversing the direction of the flow. In this case, the fluidynamic was not matched starting from the first cascade. The effect of the negative incidence present could not be accurately predicted by the meanline correlations for what concerns both thermodynamic and fluidynamic quantities. The negative incidence present due to the effects explained in section 1 is enhanced by the lower deviation angle for turbines with respect to compressors. Blades are designed for compressor deviation angle, but the lower one of turbines makes the flow more tangential. A graphic representation can be seen in Figure 6

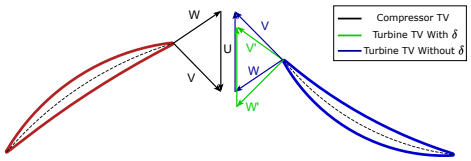

Figure 6: Velocity triangles for compressor and turbine mode

All these considerations, however, seemed not to be relevant when simulating the cascade using CFD, as can be seen in Figure 7, which represent the streamlines for the 3D simulation taken at midspan.

Figure 7: Streamlines for turbine mode.

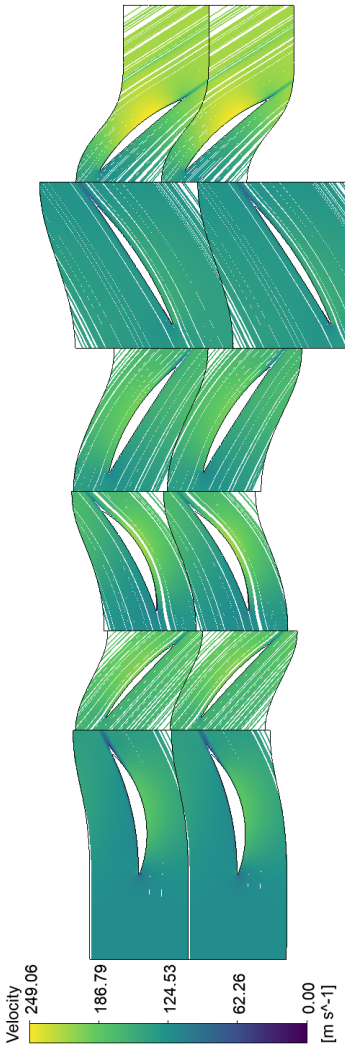

No particular effect of the incidence angle is visible, in fact CFD simulation reported a value of η_{is} of 94.3% with respect to 87.6% of the meanline code.
The significant mismatch between CFD and meanline results means that the latter cannot be used to predict accurately the machine performance. Therefore only the compressor meanline code will be used in conjunction with an optimisation routine, to obtain the final machines. The turbine mode is only analysed through CFD simulations.

3. Optimisation

Since only the compressor code is resulted reliable, the optimisation is performed solely looking at its performance. The optimisation target, therefore, is not RTE, but compressor η_{is}. The turbine mode is only analysed through high-fidelity 3D CFD simulations.
It is chosen to use the differential evolution (DE) algorithm for the optimisation routine. The main reason is the fact that DE does not require the problem to be differentiable or even continuous. Moreover, in contrast to gradient-based methods, DE avoids being trapped in local minimums. The algorithm tries different compressor designs, changing the input parameters of the meanline code (from now on referred to as optimisation variables) to find the optimal machine in terms of efficiency. Optimisation variables are the adimensional coefficients and geometrical parameters, while the thermodynamic boundary conditions are taken from an in-house code. The objective function η_{is} is lowered with some penalties in case of impossible designs or not wanted features, for example Howell limit on deflection not respected or λ too high. The optimisation is carried out for both compressor in charge mode (CC) and compressor in discharge mode (CD), for both architectures, and for both the working fluids chosen.
The full data for the four compressors are reported in Table 2.

Table 2: Input parameters for the 4 machines design optimisations.

Input	N_2 **CC**	N_2 **CD**	Ar **CC**	Ar **CD**
P_{Tin} [bar]	3.39	3.19	4.81	4.53
T_{Tin} [K]	327.93	-10.07	328.18	-4.42
P_{Tout} [bar]	10	10.63	10	10.63
$\dot{m}\left[\frac{kg}{s}\right]$	55	55	110.68	110.68
N_{st} [-]	12	12	8	8

The target power in charge is 10 MW. As explained before, β for Ar is lower, for charge mode it is of 2.08, while for N_2 is 2.95. For discharge mode it is 2.35 instead of 3.33. On the other hand, due to the lower heat capacity of Ar, $\dot{m}$ needed to match the power is higher. It is chosen a β_{TT} of around 1.1 per stage, resulting in 8 stages for Ar and 12 for N_2.
Results of the rotors and stators machine are shown in Table 3.

Table 3: Optimisation results for the rotors and stators machine.

Param.	N_2 **CC**	N_2 **CD**	Ar **CC**	Ar **CD**
D_m [mm]	/	1268	1345	1255
ϕ_1	/	0.51	0.45	0.33
ϕ_i	/	0.55	0.59	0.53
ϕ_n	/	0.71	0.73	0.75
χ_1	/	0.85	0.87	0.87
χ_n	/	0.60	0.60	0.58
λ_1	/	0.43	0.37	0.31
λ_n	/	0.20	0.21	0.20
σ_1	/	1.13	1.16	1.07
σ_2	/	1.14	1.04	1.07
σ_i	/	1.17	1.19	1.11
σ_{2n-1}	/	1.12	1.07	1.03
σ_{2n}	/	1.19	1.18	1.20
η_{is}	/	0.82	0.89	0.83

For the rotors and stators machine, the optimisation of CC with N_2 could not find an optimum after 4 days of calculations, therefore it was stopped and not considered. The other optimisations required about 2 days to find the solution. All the machines had their efficiency penalised by the first stator not increasing the pressure. This is due to the fact that the acceleration of the flow due to the axial velocity imposed by ϕ of the repeated stages compensated the increase of pressure due to the blade deflection. Moreover, it presented a reduced thickness-to-chord ratio, which in the case of the CD for Ar is below 5%. This can be a problem for the structural integrity of the blade.
The optimal D_m is a trade-off between the deflection and blade height: a lower D_m increases the deflection needed and therefore the profile losses, while a higher D_m lowers the blade height for the same $\dot{m}$, increasing end-wall losses. Moreover, due to the high D_m, the blade height was low, with a maximum value of $\frac{b}{D_m}$ of 0.043 at the inlet of Ar CC.
The results for the machine with guide vanes are reported in Table 4.

Table 4: Optimisation results for the machine with guide vanes.

Param.	N_2 **CC**	N_2 **CD**	Ar **CC**	Ar **CD**
D_m [mm]	1775.1	1306.34	1386	1301.12
ϕ	0.4249	0.4239	0.467	0.456
σ_{IGV}	1.11	1.08	1.05	1.09
σ_i	1.12	1.02	1.2	1
σ_{OGV}	1.895	1.96	1.89	1.99
η_{is}	0.867	0.849	0.896	0.84

The optimisations for the machines with guide vanes required only about 10 hours, due to the reduced number of optimisation variables. The results are similar to the one for the rotors and stators machine. However, no designs was subject to any penalty, emphasising the simpler design. Moreover, η_{is} resulted higher than the previous architecture, therefore the turbine mode is analysed only for the machines with guide vanes.

4. CFD Analysis

Once the geometries for the different machines are obtained, the turbine mode can be analysed through high-fidelity CFD simulations. The blade discretisation for grid independency resulted in around 2 000 000 cells per cascade, but due to memory limit, the total number of cells for the entire machine has to be kept at around 10 000 000.
The boundary conditions for turbine in charge mode (TC) and for the turbine in discharge mode (TD), along with the target β_{TT} are shown in Table 5.

Table 5: Boundary conditions for turbine CFD simulations.

BC	N_2 **TC**	N_2 **TD**	Ar **TC**	Ar **TD**
P_{Tin} [bar]	9.604	10	9.604	10
T_{Tin} [K]	333.176	813.762	333.386	813.246
$\dot{m}\left[\frac{kg}{s}\right]$	55	55	110.68	110.68
β_{TT}	2.72	2.95	1.917	2.079

Machines are simulated using the same $\dot{m}$ as the compressor counterpart.
The meanline prediction of the negative incidence accumulating cascade over cascade was correct, as depicted in Figure 8. The incidence on the OGV is positive due to the opposite curvature with respect to the stators.

Figure 8: Streamlines for Ar TD.

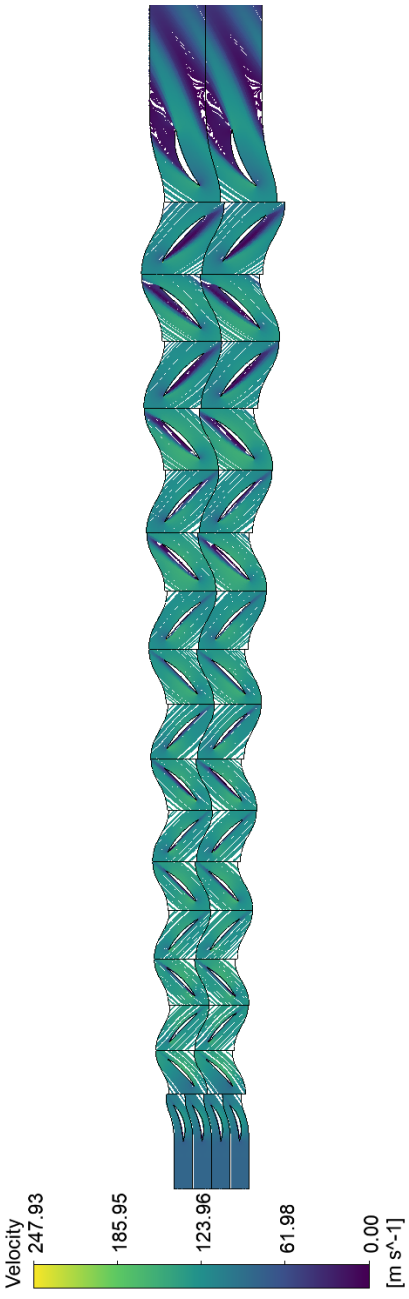

The other simulations present similar fluidynamic results, therefore it is shown only the representation of TD for Ar.
The incidence angle along the machines is shown in Figure 9.

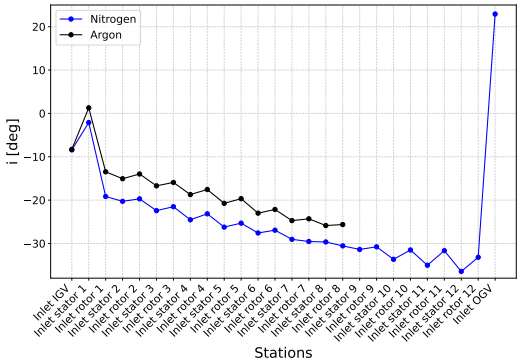

(a) TC trend of i for Ar and N_2.

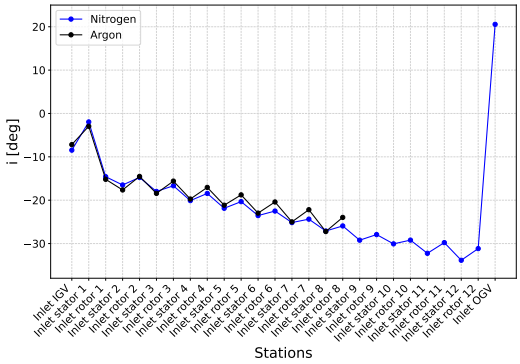

(b) TD trend of i for Ar and N_2.

Figure 9: Incidence angle trend for both turbines with both working fluids.

Incidence angle on the OGV is 14.4° for the Ar TC and 14.9° for the Ar TD.
This has the consequence of making some of the rotor rows act as compressors: incidence is so negative that the tangential velocity at the inlet of a cascade is greater than the one at the outlet, increasing P_T. This effect is visible in the λ trend for the stages, as represented in Figure 10.

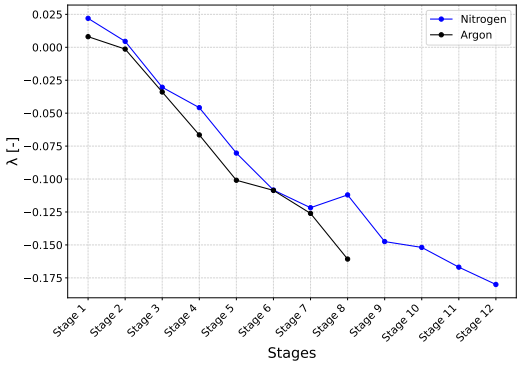

(a) TC trend of λ for Ar and N_2.

Figure 10: Work Coefficient trend for both turbines with both working fluids.

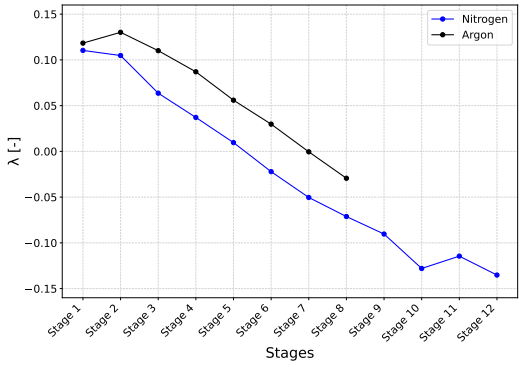

(b) TD trend of λ for Ar and N_2.

Figure 10: Work Coefficient trend for both turbines with both working fluids.

The situation is better for TD, since more stages are able to expand the flow.
This resulted in the P_T to be almost the same between inlet and outlet for TC, while TD is able to expand the flow, still not reaching the target P_{Tout}.
The trend in P_T can be seen in Figure 11.

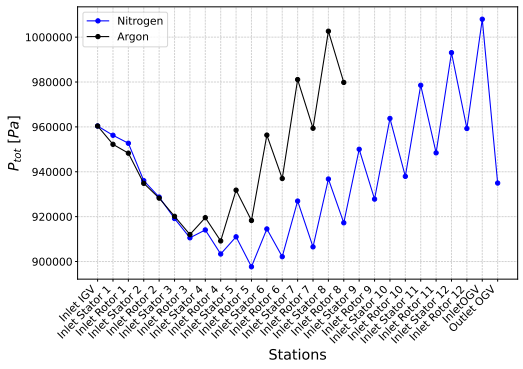

(c) TC trend of P_T for Ar and N_2.

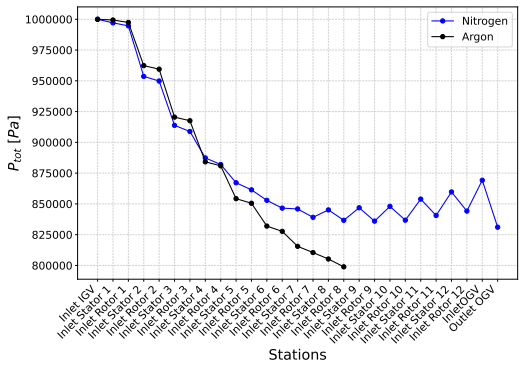

(d) TD trend of P_T for Ar and N_2.

Figure 11: Total Pressure trend for both turbines with both working fluids.

P_T at the inlet of the OGV is1 007 920 Pa for the Ar TC and 800 155 Pa for the Ar TD, while P_{Tout} is 962 834 Pa for the Ar TC and 779 833 Pa for the Ar TD.
P_T increases for rotor rows, due to the effect explained earlier and decreases in stator rows, due to the total pressure loss. Trend of the total pressure loss $\bar{\omega}$ is depicted in Figure 12.

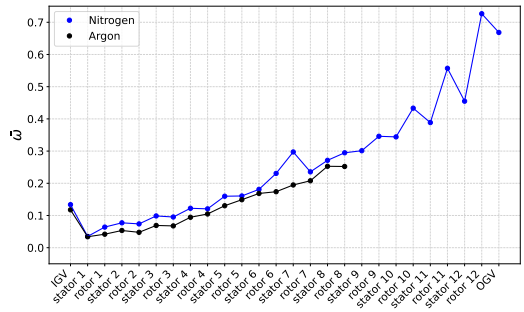

(a) TC trend of $\bar{\omega}$ for Ar and N_2.

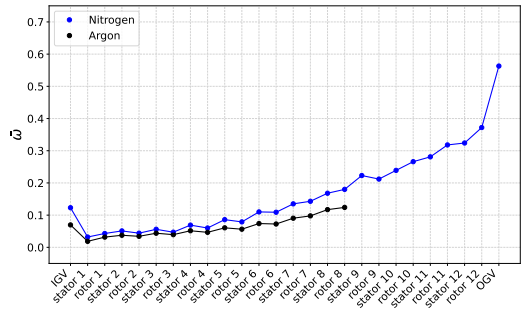

(b) TD trend of $\bar{\omega}$ for Ar and N_2.

Figure 12: Total Pressure Loss trend for both turbines with both working fluids.

$\bar{\omega}$ for OGV is 0.4533 for the Ar TC and 0.3874 for the Ar TD.
Losses present an increasing trend, as expected for the increasing incidence angle.
No machine could expand the fluid as required. P_{Tout} for TC is almost the same as P_{Tin} because of its increase in rotor rows due to work exchanged and decrease in stator rows due to total pressure losses. For TD the situation is less critical, with all the rotors expanding the flow for Ar. For N_2 only the first 7 rotors are able to expand the flow. Nevertheless, the correct P_{Tout} is not matched even in these cases. For TD Ar it is 7.79 bar compared to the theoretical 4.81 bar, while for TD N_2 it is 8.31 bar compared to 3.389 bar. However, in relative terms, the Ar machine reached 62% of the theoretical β_{TT}, while the N_2 machine only the 40%.
Overall, the two working fluids present a similar trend in all the quantities represented here. Both TC start to pressurise the flow at the third

rotor. This means that almost half of the stages for Ar act as turbine, while only a third for N_2. For both machines, Ar has also lower total pressure losses.
D_m for Ar and N_2 TC is similar (respectively 1301 mm vs 1306 mm), while it is different for TD (respectively 1775 mm vs 1386 mm). This causes the λ to be lower and both M and M_w to be higher for TD N_2. For TC λ is similar, while M and M_w present opposite trend: the Ar one is higher.
All these considerations are in favour of choosing Ar as working fluid when aiming at reversible turbomachinery: higher β_{TT}, higher percentage of stages expanding the flow and lower losses. In order to choose the working fluid, however, other considerations, such as the cost of the heat exchangers should be considered.
A way to improve the negative incidence angle is to increase $\dot{m}$. However, this is not trivial. A higher mass flow rate for discharge mode ($\dot{m}_D$) with respect to the charge mode one ($\dot{m}_C$) may be considered. By doing so, when operating in charge mode, the compressor is designed for the required $\dot{m}_C$, while the turbine is the reversed CD, which is designed for $\dot{m}_D > \dot{m}_C$. This means that TC has the geometry optimised for $\dot{m}_D$, but it operates with lower $\dot{m}$. This would increase the negative incidence problem. The opposite happens if $\dot{m}_C$ is higher than $\dot{m}_D$.

5. Conclusions

A new methodology to design and analyse reversible axial turbomachinery for the application on a closed Brayton cycle has been proposed. The main peculiarity of this kind of machine is that either compressor or turbine mode cannot operate at their optimum condition, due to different work exchanged and therefore different incidence angle.
Being a closed cycle, there is the advantage of choosing the working fluid to operate with. Two fluids were compared: N_2 and Ar. Ar allows to reduce the number of stages, while N_2 decreases the costs for the heat exchangers.
The design methodology used was to predict both operating modes functioning by developing a code base on a meanline approach. In this way, the calculations could be coupled with an optimisation routine, in order to find the geometry that maximises the RTE.
Two codes were developed, one for compressor mode, designing at its optimum conditions and one for turbine mode, analysing the compressor geometry reversing the flow direction. This choice is made since compressor functioning is more influenced by variation in the incidence angle. The codes exploit specific correlations for compressor and turbines in order to calculate total pressure losses, optimal incidence angle and deviation angle.
The codes could be coupled with the optimiser only if they resulted accurate when compared to high-fidelity CFD simulations. Comparisons were carried out and it resulted that only the compressor code resulted accurate, since it was able to match the outlet total pressure and η_{is} with reasonable accuracy (P_{Tout} obtained was of 262055 Pa, compared to 265000 Pa of the meanline code, and η_{is} was 90.5% compared to 88.6%). Turbine code, instead resulted very inaccurate, showing a complete mismatch of both P_{Tout} (209753 Pa of the simulation vs 186060 Pa of the code) and η_{is} (94.3% of the simulation vs 87.6%of the code). The significant mismatch is due to the negative incidence angle present, which effects are not well predicted by the code. In particular, deviation angle correlation does not depend on the incidence angle, but only on geometrical parameters, therefore is not able to predict accurately the actual behaviour.
Two architectures were compared: one composed by only rotors and stators, the other with guide vanes at inlet and at the outlet. Due to the low reliability of the turbine code, no guide vane rotations are implemented.
The two optimised machines provided comparable efficiencies, but the design of the one with guide vanes was not affected by design criticality. In particular, the machine composed by rotors and stators present reduced blade thickness and decreasing pressure across the first stator. η_{is} for the machines with guide vanes are of 86.7% for N_2 and 89.9% for Ar in charge mode, while for discharge mode they are 84.9% for N_2 and 84.0% for Ar. This architecture was the one chosen for analysing turbine mode.
As predicted, turbines cascade showed increasing negative incidence angles. Because of this, not only the target outlet pressure could not be reached, but some rotor rows acted as compressor cascades during the turbine mode opera-

tion. Nevertheless, *Ar* machine provided better results in terms of expansion ratio and incidence angle, showing more promising results.

5.1. Future Works

This work was the starting point for designing reversible axial turbomachinery. There are different paths that can be pursued in order to improve the design method for this kind of machines:

- improve the meanline analysis code predictions by improving turbine losses and deviation correlations. In particular, there is the necessity of including the influence of the incidence angle on the deviation angle. By doing so, also the turbine code could be coupled together with the compressor one for the optimisation routine, therefore maximising RTE, and not the single machine efficiency
- accounting for spanwise evolution at the meanline level. Flow calculations are performed using a meanline approach, but more accurate results could be obtained by including three-dimensional effects, such as solving the non-isoentropic radial equilibrium for the spanwise distribution of properties
- different design strategy. Operating the compressor at its optimum design point made the turbine work with strong negative incidence. A different spanwise design from the free-vortex method can be also envisaged
- evaluate the benefits of employing rotating IGV for turbine mode, in order to obtain design incidence angle on the first stator.
- consider different rotational speeds for the two operating modes, with the aim of mitigating the negative effects.

References

[1] European Commission. A european green deal, 2019. URL `https://commission.europa.eu/strategy-and-policy/priorities-2019-2024/european-green-deal_en#actions`.

[2] J. D. Chiapperi. Attributes of bi-directional turbomachinery for pumped thermal energy storage. Master's thesis, Massachussetts Institute of Technology, https://www.mit.edu/, 5 2021.

[3] R. Laughlin. Pumped thermal grid storage with heat exchange. *Journal of Renewable and Sustainable Energy*, 9:044103, 07 2017. doi: 10.1063/1.4994054.

[4] P. Farrés Antúnez. *Modelling and development of thermo-mechanical energy storage*. PhD thesis, University of Cambridge, https://www.cam.ac.uk/, 9 2018.

[5] P. Harris, T. Wolf, J. Kesseli, and R. B. Laughlin. An Investigation of Reversing Axial Turbomachinery for Thermal Energy Storage Application. volume Volume 5: Controls, Diagnostics, and Instrumentation; Cycle Innovations; Cycle Innovations: Energy Storage of *Turbo Expo: Power for Land, Sea, and Air*. ASME, 09 2020. doi: 10.1115/GT2020-15286. V005T07A003.

[6] R. H. Aungier. *Axial-Flow Compressors*. ASME Press, 01 2003. ISBN 0791801926. doi: 10.1115/1.801926.

[7] R. H. Aungier. *Turbine Aerodynamics: Axial-Flow and Radial-Flow Turbine Design and Analysis*. ASME Press, 01 2006. ISBN 0791802418. doi: 10.1115/1.802418.